Chemistry & Biology *13*, 129–138, February 2006 ©2006 Elsevier Ltd All rights reserved DOI 10.1016/j.chembiol.2005.11.004

Interactions of Designer Antibiotics and the Bacterial Ribosomal Aminoacyl-tRNA Site

James B. Murray,[1,*] Samy O. Meroueh,[2] Rupert J.M. Russell,[1] Georg Lentzen,[1] Jalal Haddad,[2] and Shahriar Mobashery[2,*]
[1]Vernalis (R&D), Ltd.
Granta Park
Cambridge CB1 6GB
United Kingdom
[2]Department of Chemistry and Biochemistry
University of Notre Dame
Notre Dame, Indiana 46556

Summary

The X-ray crystal structures for the complexes of three designer antibiotics, compounds 1, 2, and 3, bound to two models for the ribosomal aminoacyl-tRNA site (A site) at 2.5–3.0 Å resolution and that of neamine at 2.8 Å resolution are described. Furthermore, the complex of antibiotic 1 bound to the A site in the entire 30S ribosomal subunit of *Thermus thermophilus* is reported at 3.8 Å resolution. Molecular dynamics simulations revealed that the designer compounds provide additional stability to bases A1492 and A1493 in their extrahelical forms. Snapshots from the simulations were used for free energy calculations, which revealed that van der Waals and hydrophobic effects were the driving forces behind the binding of designer antibiotic 3 when compared to the parental neamine.

Introduction

The bacterial ribosome is an important target for antibiotics [1]. The recent availability of crystal structures for the 30S and 50S subunits of the bacterial ribosome and that of the complete 70s ribosome (reviewed in [2]) has created the possibility for de novo design of molecules that bind to the ribosome and disrupt its function. We recently disclosed a set of antibiotics that were designed to bind to the ribosomal aminoacyl-tRNA site (A site) [3]. These antibiotics were the outcome of a computational search of three-dimensional molecules for binding to the A site and their ultimate chemical syntheses, which were discussed at length previously [3]. These molecules were shown to bind to a model of the A site in solution, and, in one case, we recently reported a brief communication of the X-ray structure for the complex of the A site model and the antibiotic [4].

Three of these designer antibiotics are compounds **1**, **2**, and **3** (Figure 1A), which are the subjects of this report. We disclose herein a set of biochemical analyses with these antibiotics that reveal the various nuances of their properties. Furthermore, X-ray structures for these molecules with the model of the A site, along with one with the 30S ribosomal subunit, reveal the binding modes of the antibiotics at the target site. In addition, molecular dynamics simulations were carried out on two of these complexes, and snapshots were used to carry out free energy calculations for the binding of neamine and antibiotic **3** to the A site. Valuable insight into the driving forces behind the binding of these antibiotics was arrived at as the van der Waals, electrostatics, hydrophobic, and entropic components of the free energy of binding are determined individually. Analyses also shed light on the differences in molecular dynamics experienced by the surrounding RNA bases in the presence of two of these antibiotics. It appears that the two arms incorporated into the designer antibiotics serve as electrostatic anchors, which are the structural reasons for additional stability of bases A1492 and A1493 that adopt an extrahelical conformation. The simulations also reveal that these bases are highly flexible in solution, and that they sample a wide variety of conformations.

*Correspondence: j.murray@vernalis.com (J.B.M.); mobashery@nd.edu (S.M.)

Results and Discussion

We had presented data on the broad spectrum of the antibacterial activity that compounds **1–3** exhibited in the original disclosure of these antibiotics [3]. Also, we had shown by a fluorescence analysis that these antibiotics bind to a model of the bacterial ribosomal A site. We report, herein, the X-ray structure of antibiotic **1** bound to the A site in the 30S subunit of the ribosome of *Thermus thermophilus* at 3.8 Å (data processing and refinement statistics are presented in Table 1 for this and all other structures reported in this work). Furthermore, we report the structures of **1**, **2**, and **3** and that of the neamine core bound to a model A site RNA construct. These structures range from 2.5 to 3.0 Å resolution and reveal in detail the molecular interactions made by these antibiotics. We will use the *Escherichia coli* numbering scheme throughout in describing the structure.

The A site model constructs contain two identical A site motifs, separated by four GC base pairs, each of which closely duplicates the three-dimensional structure of the A site in the ribosome. As an aid to optimize the crystallization conditions, we have used two constructs that differ only by the overhanging residues, UU (construct 1) and C (construct 2) (Figure 1B). The best diffracting crystals were obtained by using construct 1 for antibiotic **1** and neamine, and construct 2 for antibiotics **2** and **3**. Two distinct crystal-packing arrangements were observed (Figure 1B). Type 1 was obtained for antibiotic **1** and is similar to those previously reported [5]. The remaining three antibiotics exhibit a new crystal-packing arrangement (Type 2). For both packing arrangements, only one of the sites contains an antibiotic with the empty sites involved in crystal-packing interactions that prevent its occupation by the antibiotic.

The crystal packing around the binding site for antibiotic **1** (Type 1) is similar to those reported previously [5]. Briefly, A1492 and 1493 adopt an extrahelical conformation packing in the minor groove of a neighboring molecule. The empty site is less well ordered. The adenine bases of A1492 and A1493 are completely disordered, with only weak density present for the ribose moieties.

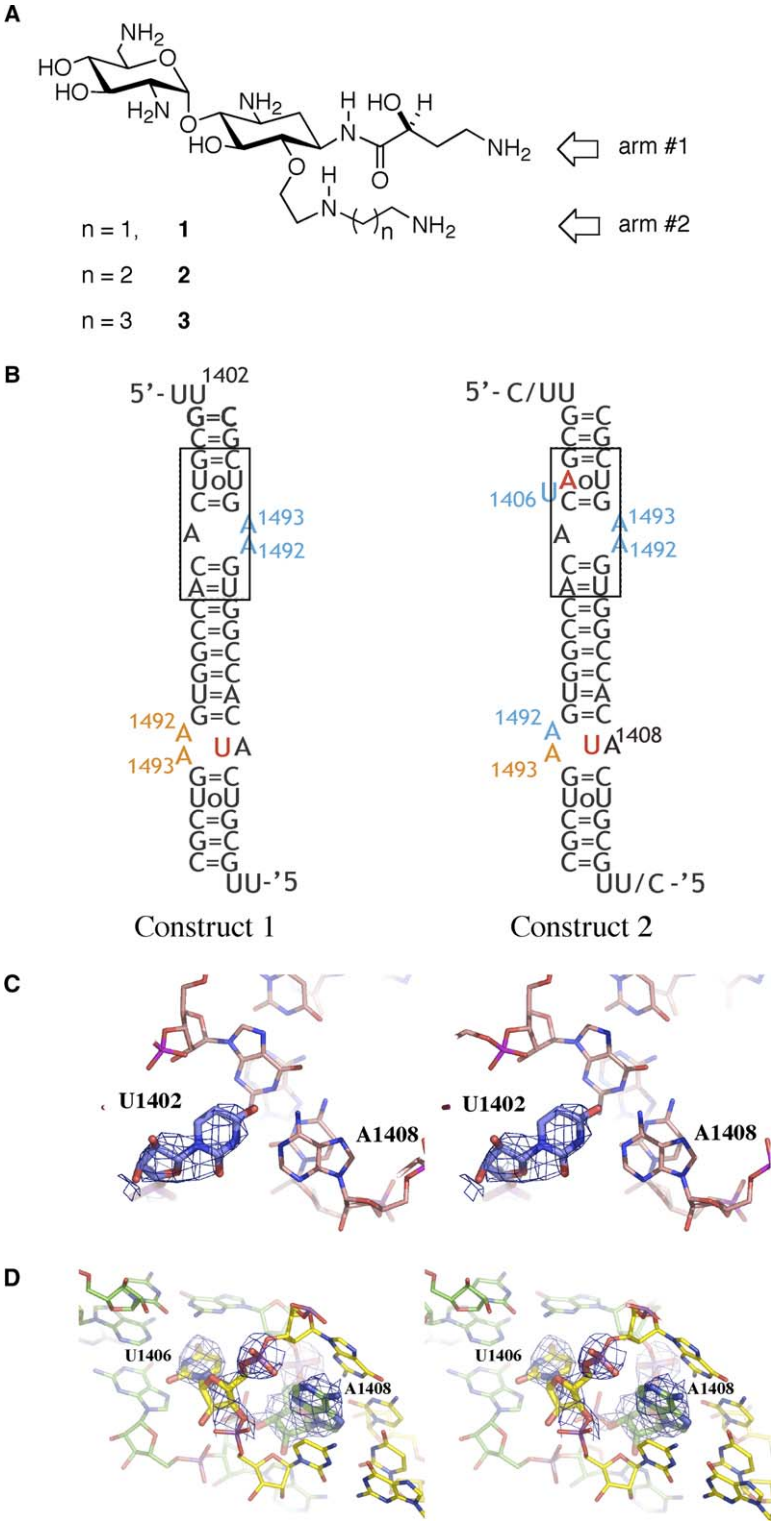

Figure 1. Antibiotic Structures and Crystal Packing Interactions for Model A Site

(A) A schematic of compounds **1–3.**

(B) Illustration of the two packing types observed; Type 1 with construct 1, and Type 2 with either construct 1 or 2. Red residues represent base pairing from symmetry mates. Gold residues are largely disordered, and blue residues are the well-ordered extra-helical elements making crystal contacts. The box represents the site of antibiotic binding.

(C) The interaction of U1402 (slate) from a symmetry mate with A1408 (salmon) in the empty site for packing Type 1. The electron density is only shown for U1402, contoured at 1σ ($2F_o - F_c$).

(D) The interaction of U1406 (yellow) with a symmetry mate, A1408 (green), to form an AU base pair, and, A1492 (green) from the same symmetry mate forming the Hoogsteen AU base pair with U1495 (yellow) for packing Type 2. The electron density is only shown for U1406 and A1408, contoured at 1σ ($2F_o - F_c$).

The electron-rich phosphates of A1492 and A1493 can be located, but, again, the density is only present at much lower contour levels than in the core of the structure. This may reflect the lack of order present in the A site, until mRNA or an antibiotic is bound, as has been observed in the structures of unliganded 30S subunits [6]. An interesting feature in this structure is the crystal contact made by U1402 (the first overhanging U, Figure 1B, construct 1, Type 1) extending into a neighboring empty site and making a UA base pair with A1408. The density for this residue does not define the orientation of the residue unambiguously, but it is clear and returns after generation of a simulated annealing omit map for this residue. Attempts to refine either of the disordered A1492 or A1493 residues into this density proved less than satisfactory; thus, the most reasonable

Table 1. Data Processing Statistics and Refinement Statistics

	Antibiotic 1	Antibiotic 1-30S	Antibiotic 2	Antibiotic 3	Neamine
Space group	$P2_1$	$P4_12_12$	$P2_12_12_1$	$P2_12_12_1$	$P2_12_12_1$
Cell parameters	a = 46.52 Å; b = 32.97 Å; c = 46.00 Å; 90, 95.62, 90	a = 403.32 Å; b = 403.32 Å; c = 176.69 Å	a = 33.052 Å; b = 46.461 Å; c = 89.524 Å	a = 32.80 Å; b = 46.55 Å; c = 88.81 Å	a = 33.055 Å; b = 47.31 Å; c = 85.34 Å
Outer shell	3.11–3.0 Å	3.93–3.80 Å	2.69–2.60 Å	2.59–2.50 Å	2.93–2.80 Å
Unique reflections	2,795	138,452	4,451	4,719	3,221
Completeness (%)	97.7 (100)	97.4 (96.2)	97.6 (97.6)	94.2 (98.2)	89.7 (85.8)
Redundancy	3.6	3.1	3.1	6.1	4.7
R_{merge} (%)[a]	7.8 (20.6)	16.1 (68.0)	9.2 (42.3)	6.6 (39.4)	7.9 (32.7)
$I/\sigma(I)$	8.0 (3.2)	8.2 (1.9)	5.8 (1.6)	16.0 (3.5)	8.1 (2.3)
Reflections	2,515 (work set); 280 (test set)	131,434 (work set); 6,940 (test set)	3,845 (work set); 445 (test set)	4,242 (work set); 477 (test set)	2,916 (work set); 305 (test set)
Resolution range	15.0–3.0 Å	30.0–3.8 Å	30.0–2.6 Å	30.0–2.5 Å	30.0–2.8 Å
RNA atoms	932	32,391	892	892	900
Ligand atoms	34	34	35	36	21
Protein atoms	—	19,078	—	—	—
Solvent atoms	0	0	31	62	13
Metallic atoms	—	114	—	—	
R factor work[b]	21.1%	25.9%	25.00%	24.6%	22.5%
R_{free}	26.7%	31.5%	29.89%	29.8%	24.9%
Average B factor	80.2 $Å^2$	84.9 $Å^2$	55.6 $Å^2$	46.9 $Å^2$	59.9 $Å^2$
Rmsd bond lengths	0.006 Å	0.019 Å	0.015 Å	0.006 Å	0.004 Å
Rmsd bond angles	0.99°	1.64°	1.97°	1.05°	0.92°
Average radial error <u>[c]	0.45 Å	0.56 Å	0.46 Å	0.42 Å	0.47 Å

[a] $R_{merge} = \Sigma |I(k) - \langle I \rangle| / \Sigma I(k)$, where I (k) is the value of the k_{th} measurement of the intensity of a reflection, <I> is the mean value of the intensity of that reflection, and the summation is over all measurements. The values in parentheses refer to the highest-resolution shells.
[b] R factor = $\Sigma_{hkl} |F_o(hkl) - F_c(hkl)| / \Sigma_{hkl} F_o(hkl)$.
[c] Average radial error, <u>, of coordinates derived from the Luzzati plot as implemented in sfcheck, part of the CCP4 suite of programs [7].

explanation is the crystal-packing interaction described (Figure 1C).

A feature of Type 2 crystal packing is the displacement of U1406 from its UU base pair to an extrahelical conformation and the formation of an AU Hoogsteen base pair when A1492 from the empty site of a neighboring molecule replaces U1406 (Figure 1D). Furthermore, the displaced U1406 stacks upon A1491 of the empty site and forms a weak base pair in the empty site with A1408, thus mimicking a Type 1 crystal-packing interaction. A1492 and 1493 adopt an extrahelical conformation and make a number of minor groove contacts with a neighboring molecule.

The crystal structure of antibiotic **1** in the 30S subunit represents the first structure of a designer antibiotic bound to its natural ribosomal target and confirms our observations when the model A site RNA constructs are used. Even though the resolution for this structure is relatively low, it shows clearly the orientation of the antibiotic with density extending partially along arms #1 and #2 (Figure 2A). Furthermore, the two codon-anticodon-sensing adenosines A1492 and A1493 have adopted an extrahelical conformation similar to that observed in all model A site-aminoglycoside structures. This is consistent with the structures determined by Ramakrishnan and coworkers of paromomycin in the 30S subunit [7]; this group's subsequent work has shed light on the mechanism of action by A site binding antibiotics [2]. In the apo 30S structures, A1492 and A1493 are not observed in an extrahelical conformation. It is also notable that we could not identify any electron density consistent with alternative binding sites in the 30S subunit for antibiotic **1**, thus indicating that these compounds are specific for the A site.

Comparison of the two structures for antibiotic **1** (in the 30S subunit and in the model A site RNA construct) shows that the structures are the same, validating the use of the A site model. The rmsd between the two structures when using common residues (U1404 to C1409 and G1491 to U1497) is 1.1 Å (0.84 Å for main chain, ribose, and phosphate). The superposition of the two structures is shown in Figure 2B.

The 2.5 Å crystal structure of the A site RNA construct in complex with antibiotic **3** unambiguously defines the precise location for all atoms of antibiotic within the A site, as previously communicated [4]. The structure of antibiotic **2** within the A site revealed that the last two atoms of arm #2 are not well defined by the electron density. Antibiotic **1** has the neamine core and arm #1 (substitution at N1 of neamine) in the same positions as those of antibiotics **2** and **3**. The shorter arm #2 of antibiotic **1** (substitution at O6 neamine) does not point down the major groove, but, rather, it continues orthogonal to the helical axis. This allows the terminal amine to make hydrogen bonds with the phosphates of C1404 and G1405 at 3.0 and 3.2 Å, respectively. Furthermore, the displaced U1406 stacks upon A1491 and forms a weak base pair in the empty site with A1408, thus mimicking a Type 1 packing interaction.

Neamine is representative of a moiety present in many aminoglycosides that bind to the A site, and it is the core structure on which we have based our design efforts. To ensure that the binding of this core is not different than that observed in larger aminoglycosides, we have

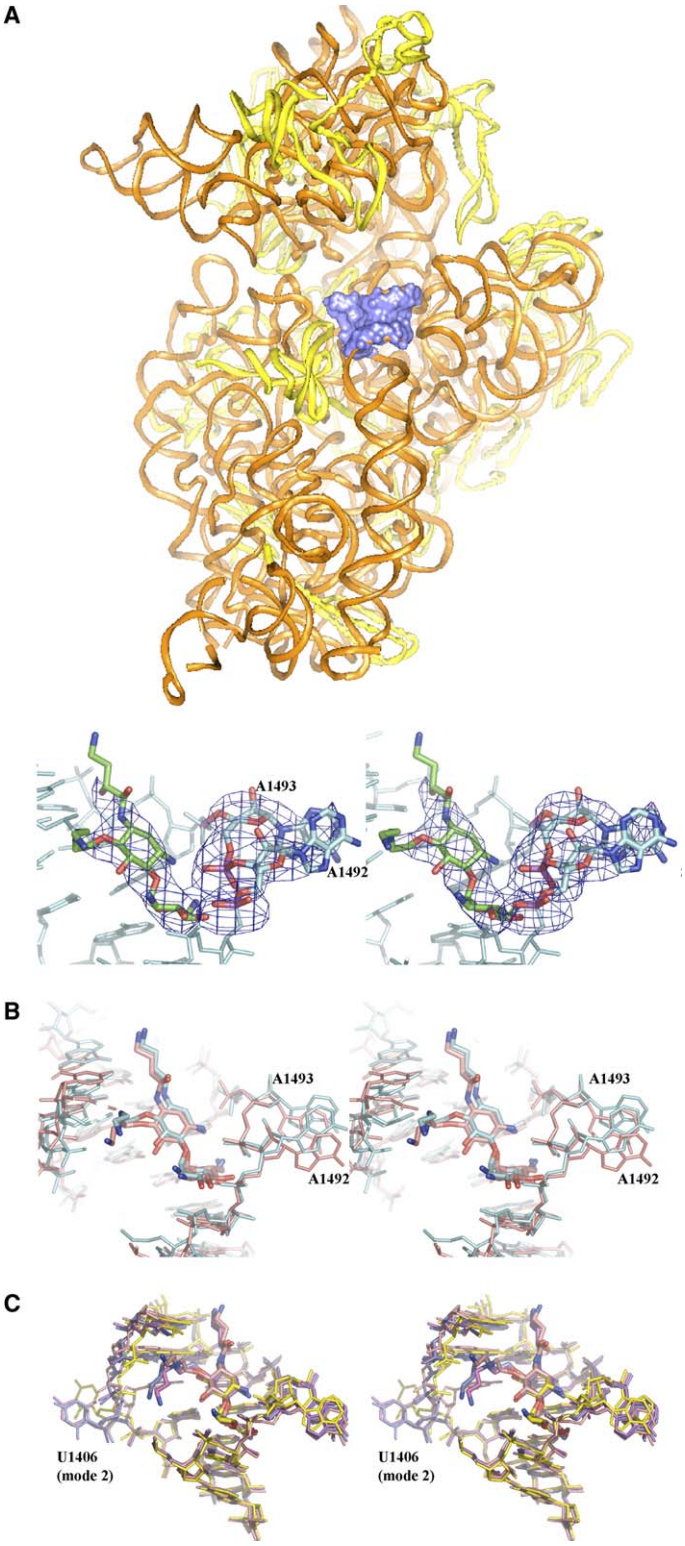

Figure 2. Structure of Antibiotic **1** Bound to the 30S Subunit and Model A Site Antibiotic Structures

(A) Top. The cartoon shows the full structure of the 30S subunit; the RNA chain is shown in gold, and protein chains are shown in yellow. The liganded A site is highlighted in blue. Bottom. Stereoview of antibiotic **1** (green) and the displaced A1492 and A1493 (cyan) in the 30S subunit. The electron density shown is the difference density ($F_o - F_c$) contoured at 3.5 σ. The antibiotic and bases A1492 and A1493 were omitted from the phasing model. This unambiguously reveals the orientation of antibiotic **1**, which is entirely consistent with that observed in the model A site construct. This also shows that A1492 is less well defined than A1493.

(B) Superposition of the binding sites for antibiotic **1** from 30S (cyan) and the A site construct (salmon). The binding mode is essentially identical, and the largest difference is seen in the orientation of the base of A1492, which, as noted above, is the least well defined part of the binding site in the 30S subunit.

(C) A superposition of all four structures. The color scheme is as follows; antibiotic **1**, **2**, and **3** and the neamine core are colored salmon, purple, blue, and yellow, respectively. The superposition was calculated from all atoms by using residues 1407–1410 and 1490–1495. This figure also illustrates the flipping out of U1406 for packing Type 2.

solved the structure of neamine in the A site at 2.8 Å. The neamine core alone binds in the same manner as that observed in the other structures reported. With residues 1407–1410 and 1490–1495, the rmsd between the structures for antibiotic **1**, **2**, and **3**, and the neamine core are 0.26, 0.39, and 0.31, respectively. This is illustrated in Figure 2C. In light of the fact that the neamine core is devoid of antibacterial activity, it is the two arms of antibiotics **1**–**3** that are responsible for the dramatic antibacterial activity. It is worth mentioning that the arms might also be important in the uptake of the antibiotics by bacteria.

The aminohydroxybutyryl group that forms arm #1 has the same structure in the three complexes (**1**–**3**) with the

Table 2. Free Energy of Binding for the Formation of the Complexes between A Site and Compound **3** or Neamine

	ΔE^{vdW}	ΔG^{elec}	ΔG^{surf}	$T\Delta S$	ΔG^{calc}	ΔG^{exp}
Compound **3**	−35.0 ± 0.9	−13.5 ± 0.6	−4.8 ± 0.1	−45.6 ± 1.2	−7.7 ± 1.6	−7.4
Neamine	−20.0 ± 0.6	−15.0 ± 0.3	−3.4 ± 0.1	−31.6 ± 1.2	−6.8 ± 1.4	−6.5

All energies are given in kcal/mol. ΔE^{vdW}, van der Waals potential energy; ΔG^{elec}, electrostatic energy and electrostatic contribution to the solvation free energy; ΔG^{surf}, nonpolar contributions to solvation free energy; ΔS, entropy; ΔG^{calc}, change in the calculated free energy of binding; ΔG^{exp}, change in the experimentally determined free energy of binding calculated from the dissociation constants.

A site RNA model. The arm makes four contacts with the RNA. These interactions are dominated by involvement of the terminal amino group, which contacts the bases of G1403, G1498 (via water), and C1497. The hydroxyl group makes a water-mediated contact to the phosphate backbone of U1495.

Arm #2 adopts different conformations in each of the three antibiotics. For arm #2 of antibiotics **2** and **3**, the secondary amine makes a hydrogen bond with the N7 of G1405. Antibiotic **1** does not make this hydrogen bond with N7 of G1405, but it has the NH rotated 90° down the helix. This rotation allows the terminal amine to make the more favored electrostatic interactions described below. Antibiotic **3** has the methylene hydrogens spaced between the phosphate backbone of residues C1404, G1405, and U1406. The terminal amino group also makes electrostatic interactions with the phosphate groups of G1405 and U1406. The lower resolution for the structure of antibiotic **2** makes definitive conclusions about the orientation of this flexible arm difficult; however, refinement of the structure leaves the C1 and C2 positions of the aliphatic portion of arm #2 rotated by approximately 110° toward the RNA. This allows the less well-ordered atoms to adopt a conformation that is similar to that of antibiotic **3**.

Molecular dynamics simulations provide coordinates and momenta of atoms with respect to time, and they thus enable us to make a detailed study of the various conformations sampled by a system. Furthermore, molecular dynamics simulation between complexes of proteins and nucleic acids and small molecules could be used to determine the free energy of binding of these molecules to their binding sites; one such method is known as MM-PBSA [8], which combines polar and nonpolar contributions to the solvation free energy, energies from electrostatic and van der Waals interactions, and entropy calculations. This method has been extensively used for protein-ligand complexes, and, less commonly, it has been used for nucleic acid-ligand complexes. Here, the MM-PBSA method is used for the first time to probe the binding of aminoglycoside derivatives to the A site of the ribosome. Two separate molecular dynamics simulations were carried out; one for neamine and another for antibiotic **3**, each bound to the A site RNA model (by using construct 2 [Type 2], see Figure 1B).

The computed binding free energy and its components are listed in Table 2 for neamine and antibiotic **3**, respectively. The binding free energies (ΔG^{calc}) are in good agreement with experiment (ΔG^{exp}), and they also reproduce the experimental observation showing neamine with a larger dissociation constant. Comparison of the individual components listed in Table 2 reveal that van der Waals interactions (ΔE^{vdW}) provide significant stabilization to antibiotic **3** and neamine. However, it appears that these effects play a more important role in the binding of antibiotic **3** by 15 kcal/mol. This is likely due to the high degree of complementarity between the arms of the designer compound (not present in neamine) and the A site pockets they were intended to target. The electrostatic contributions to free energy of binding (ΔG^{elec}), which combine the electrostatic interactions and the solvation free energy determined by Poisson-Boltzmann electrostatics, also provide additional stability to the formation of the complex between these compounds and the A site. However, the role of electrostatics appears to be more significant, by approximately 1.5 kcal/mol, in the case of binding of neamine as opposed to antibiotic **3** (this despite the hydrogen bonding interactions between the arms of antibiotic **3**—not present in neamine—and the receptor site). This result is likely due to the penalty incurred for desolvating antibiotic **3**, as the additional charged amino groups in the arms of antibiotic **3** likely form highly favorable interactions with the solvent. The favorable hydrogen bonding interactions between compound **3** and the receptor site are not sufficient to offset this desolvation penalty. Furthermore, the hydrophobic component of the solvation free energy (ΔG^{surf}) is more favorable, by 1.4 kcal/mol, for antibiotic **3**, likely as a result of the aliphatic groups in the arms of antibiotic **3**, which prefer the binding pocket of the A site that is partly shielded from water. Finally, entropy (ΔS) appears to play a destabilizing role for the binding of antibiotic **3** and of neamine. However, a more significant penalty is incurred in the case of antibiotic **3**, as the arms of this compound introduce a larger degree of disorder in the solvent (not present in neamine), which will be lost due to binding to the A site. The larger degree of stabilization required to bind antibiotic **3** to the A site pocket will lead to a larger entropy cost. It thus appears that van der Waals interactions and the hydrophobic component of the solvation free energy of binding are the main driving forces behind the binding of the designer antibiotics over neamine. This is due to a high degree of complementarity between the arms of the designer antibiotic, which fit well into the receptor subsites they were designed to exploit.

To study the degree of flexibility exhibited by these systems, base-averaged fluctuations were determined from snapshots collected at 0.2 ps intervals during the course of the 1.8 ns trajectories, as shown in Figure 3A. The peaks around bases C1498, G1403, G1414, and C1486 are typical of terminal bases, which exhibit more flexibility, due to the fact that they form only one-sided stacking interactions while being fully exposed to solvent on the other side. Another peak in the fluctuation of U1406 is consistent with the fact that this base has an extrahelical conformation and could freely undergo motion in the solvent. The region between A1492 and

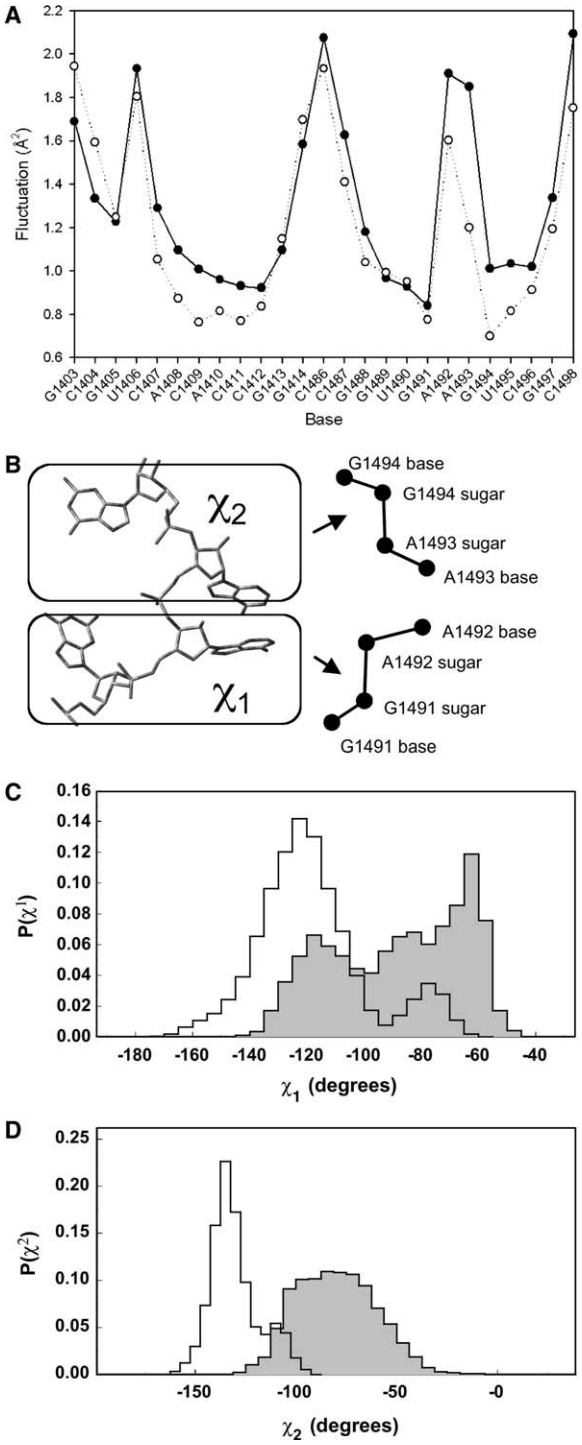

Figure 3. Dynamics of Bases in the Presence of Neamine and of Antibiotic **3**

(A) Base-averaged fluctuation of bases from the molecular dynamics simulations of neamine (closed circles) and antibiotic **3** (open circles), each bound to the A site model.

(B–D) (B) Definition of pseudo dihedral angles χ_1 and χ_2. Distribution of the pseudo dihedral angles χ_1 and χ_2, as defined in (B), from the molecular dynamics simulation for χ_1 (see [C]) and χ_2 (see [D]) in complex with the A site model. Values for neamine are shaded.

A1493, which shows larger flexibility in the neamine simulations, is of interest, given the important role that has been attributed to these bases in the process of translation. A peak in the fluctuation at positions A1492 and A1493 is due to the extrahelical conformations adopted by these bases, leading to more significant motion due to the lack of base pairing and stacking interactions. However, it is interesting to note that the fluctuations experienced by A1493 in the neamine complex were larger than those experienced by A1493 in the complex with antibiotic **3**, with a difference of 0.7 Å^2.

The motion of bases A1492 and A1493 from the intrahelical to extrahelical positions in the A site would appear to be significant in the translation process [9, 10]. An important outcome in translation is the high fidelity of the transmission of the sequence information from mRNA to the nascent protein sequence during the events of molecular recognition between codon and anticodon of mRNA and tRNA, respectively. Ramakrishnan recently documented that in the ternary complex of the 30S ribosomal subunit with fragments of RNA involved in the codon-anticodon recognition events, the A1492 and A1493 were trapped in the extrahelical positions, such that the bases were interacting with the codon-anticodon entities [9]. The authors argued that these extrahelical interactions played a key role in discrimination against binding by noncognate or near-cognate tRNA molecules, proposed also by Yoshizawa and coworkers [10]. It is known that binding of aminoglycoside antibiotics at the ribosomal A site increases the rate of misincorporation of amino acids during translation, which ultimately leads to the demise of bacteria [11]. In light of the fact that the same extrahelical positions for A1492 and A1493 have been seen when aminoglycosides bind the A site [7, 12], the point was made that, in the presence of aminoglycosides, the higher rate of amino acid misincorporation takes place because near-cognate or noncognate tRNA molecules are increasingly recognized as cognate tRNA, hence contributing to high error rates. The conformational change experienced by A1492 and A1493 in the presence of aminoglycosides was further corroborated by fluorescence labeling experiments carried out in the Pilch [13, 14] and Hermann [12] laboratories that revealed that ligand binding to the A site induces conformational change at A1492 and A1493.

Given the importance in the proposed role that A1492 and A1493 play in the decoding process, further comparison of the flexibility of these bases in the presence of neamine and of antibiotic **3** was made. To quantify the degree of extrahelical conformational change that these bases undergo, pseudodihedral angles, akin to those recently used in a DNA simulation [15], were defined, as shown in the inset of Figure 3B. These angles were defined by using bases G1491/A1492 (χ_1) and bases A1493/G1494 (χ_2). To put these angles in perspective, χ_1 and χ_2 are determined from the recently solved X-ray structure of the 30S ribosome with no antibiotic bound to the A site [6] with fully stacked intrahelical A1492 and A1493, and from the X-ray structure of the 30S ribosome with antibiotic **1** bound to the A site depicting the extrahelical bases; these angles were found to be 5° and −9° when the bases are fully stacked intrahelically, and −135° and −256° for the extrahelical conformations. The distributions of χ_1 and χ_2 are shown in

Figures 3C and 3D. When antibiotic **3** is bound to the A site, χ_1 ranges from −60 to −175, compared with −44 to −147 when neamine is bound. The distribution of χ_1 angles, however, is narrower in the case of antibiotic **3**, as reflected by a full width at half-maximum of 30°, as opposed to 60° for neamine. The majority of the χ_1 angles adopted by A1492 when antibiotic **3** is bound are within 20° of −120, the mean value. When neamine is bound, the distribution of χ_1 values is more uniform. The distributions of χ_2, as shown in Figure 3D, indicate a similar trend, but there appears to be much less overlap in the distributions. The full width at half-maximum for antibiotic **3** is 20°, compared to 60° for the neamine complex. The distributions of χ_1 and χ_2 angles reflect the differences between the motions experienced by A1492 and A1493 in the presence of neamine or of antibiotic **3**. It appears that antibiotic **3** has a stabilizing effect on the bases, favoring the extrahelical conformers. In the presence of neamine in the A site, A1492 and A1493 seem to prefer conformations of the bases that are closer to the stacked intrahelical positions, while also exhibiting equal probabilities of adopting extrahelical conformations, as evidenced by the more uniform and broad distributions of χ_1.

To illustrate the differences in the conformational changes that A1492 and A1493 experience in the presence of neamine and of antibiotic **3** in the complexes, snapshots were collected at 100 ps intervals along the 1.8 ns dynamics trajectory, as shown in Figure 4. In the X-ray structure of the A site RNA model, U1406 is shown to adopt an extrahelical conformation due to interactions between neighboring RNA molecules in the crystal lattice. One interesting aspect of the dynamics simulation with antibiotic **3** is the fact that U1406 is found to move gradually into the minor groove and finally adopt its native intrahelically stacked conformation, culminating in the hydrogen bond formation between O4 of U1406 and N3 of U1495. At the beginning of the trajectory, the O4-N3 distance was 14 Å. The distance gradually decreases during the first 200 ps of the simulation, reaching an average value of 2.7 Å over the remaining 1.6 ns of simulation. Figure 4 also illustrates that A1492 and A1493 experience more flexibility when neamine is bound. In contrast, the bases appear to be stabilized in an extrahelical position by the presence of antibiotic **3** in the A site. The differences between the structures of the neamine core and of antibiotic **3** center on the two arms, which provide the stabilizing effect for the complex of **3** bound at the A site. The two arms serve as electrostatic anchors by the formation of hydrogen bonds with the A site RNA. These anchors provide additional stability to the extrahelical conformation of bases A1492 and A1493. This added stability is likely the basis for the potent antimicrobial activity of compound **3** in light of a recent study showing that the antimicrobial activity of paromomycin is rooted in its ability to lead to destacking of these bases [13, 14].

We have also carried out a series of functional and binding analyses. These results are summarized in Table 3. While there is some correlation between the binding data and translation inhibition, this is not absolute and does not hold up for the parental molecule neamine of these series, which is a weak A site binder (K_d = 19 μM) [3], but a potent inhibitor of bacterial translation

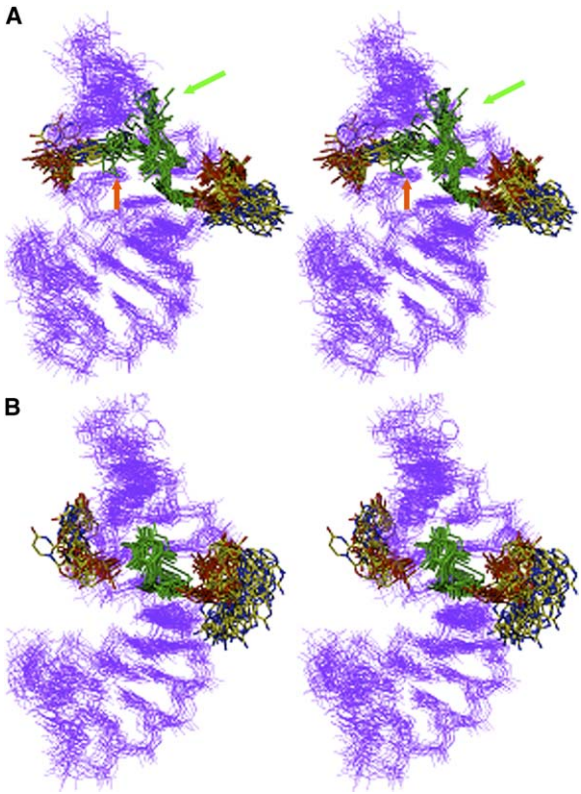

Figure 4. Illustration of Base Motion in the Presence of Neamine and of Antibiotic **3**

Superimposition of snapshots collected along the 1.8 ns molecular dynamics simulation at 200 ps intervals of (A) antibiotic **3**, with green and orange arrows pointing to arms #1 and #2 of the antibiotic, respectively, and (B) neamine bound to the A site model.

(IC_{50} = 0.13 μM; see Table 3). The likely explanation for this is that these compounds are transported into the cytoplasm in an energy-driven process that could proceed against a concentration gradient. A site binding was assayed in an alternative fluorescence assay by using a fluorescently labeled A site RNA and paromamine, and the decrease in fluorescence resonance energy transfer (FRET) upon competition of a test compound at 500 μM was measured [16]. In this assay, all compounds (**1–3**), including amikacin, were active, whereas neamine showed less than 50% inhibition, which correlates with its comparably weak antibacterial activity. Antibiotics **1–3** have similar affinities for the A site RNA, and all show similar antibacterial activities and no cytotoxicity (at >100 μM). Antibiotic **1** is the poorer of the three antibiotics in bacterial susceptibility testing [3]. It is also a weaker inhibitor of in vitro translation, it does not inhibit translation in the more stringent MS2 bacterial translation assay, and it lacks selectivity for bacterial over mammalian translation. Antibiotics **2** and **3** do show selectivity in the in vitro translation assays. Furthermore, since they are nontoxic to the HeLa cells at concentrations above 100 μM, it would appear that they do not readily penetrate the mammalian cells to manifest any potential inhibition of the translation machinery. The results of the stringent MS2 activity assay are interesting in light of the fact that antibiotics **2** and **3** would appear to be superior to amikacin (which shows

Table 3. Summary of Compound Properties

Antibiotic	A Site K_d[a]	*E. coli* IVT IC_{50}	RRL IVT IC_{50}	SI	MS2 Activity	MIC	CC_{50}
1	2.2 ± 0.1	38 ± 2	17 ± 0.3	0.4	—	0.8	>100
2	5.9 ± 1.3	3 ± 2	30 ± 2	10	+++	0.8	>100
3	3.9 ± 0.1	4 ± 3	23 ± 3	6	+++	0.8	>100
Neamine	19 ± 1	0.13 ± 0.04	55 ± 3	423	+++	12.5	>100
Amikacin	n.d.	0.013 ± 0.001	>50	>3846	++	3	>100

With the exception of the values for the selectivity index (SI) and the MS2 activity, which are unitless, all other numbers are expressed in μM. SI is the selectivity index for *E. coli* IVT IC50 versus RRL IVT IC50.
[a] A site K_d from [3].

>50% inhibition at 200 μM), a clinically used aminoglycoside antibiotic. We state parenthetically that antibiotics **1–3** did not inhibit DNA replication and transcription, indicating that their antibacterial activity is due to inhibition of translation.

Significance

The three-dimensional structures of a set of three designer antibiotics and their core structural components (neamine) have been disclosed. Furthermore, for the first time, the crystal structure of a designer antibiotic (antibiotic 1) bound to the decoding site of the 30S subunit of the ribosome has also been reported herein. These structures reveal that the A site bases A1492 and A1493 undergo a conformational change upon binding of the designer antibiotics similar to those of other A site binding antibiotics and also to the events during the translation process. The arms incorporated synthetically to the antibiotics are responsible for their antimicrobial activity, a finding that has important implication for the future design of novel antibiotics targeting the A site. Extensive molecular dynamics simulations, starting with the X-ray structures of neamine and antibiotic 3 bound to the A site, revealed that the dynamics experienced by the A1492 and A1493 bases are distinct, with the designer antibiotic found to introduce additional stability to the RNA bases. Additional molecular dynamics-based free energy calculation revealed that van der Waals and hydrophobic components are the main driving forces behind the binding of the compounds to the A site.

Experimental Procedures

Antibiotics **1–3** were synthesized by the reported procedures [3].

Crystallization, Data Collection, and Processing and Structure Refinement

Crystallization of the 30S subunit [17] and the model A site construct [4] was performed as previously described. Data were collected at ESRF on ID29 for antibiotic **1** complexed with the 30S subunit. We included demeoxycycline at the same concentrations during the 30S soaking experiments as an internal standard; we observed good ligand density at similar contour levels to antibiotic **1**. The model A site data were also collected at ESRF on ID29 for neamine and antibiotics **1** and **3**; data for the complex with antibiotic **2** were collected by using a rotating anode RU 300 coupled with an RAXIS IV++ area detector. The data were processed and scaled with the HKL2000 suite [18]. With the model A site construct, molecular replacement solutions were found by using Molrep [19] with the structure of Vicens and Westhof [5] (PDB ID 1J7T) or the structure of the complex of antibiotic **3** (PDB ID 1O9M) [4] as the search model. The 30S subunit structure was refined with Refmac5 [19] with the unliganded 30S structure as the starting model (PDB code 1J5E), whereas the model A site structures were refined with CNX [20]. Where required, the models and ligands were manually built with O (Table 1) [21].

Functional and Binding Assays

In vitro translation (IVT) assays were essentially performed as described earlier [22]. Bacterial translation was measured in a microtiterplate-based coupled transcription/translation assay by using *E. coli* S30 extracts [23] and by using firefly luciferase DNA (Promega) as a template for transcription/translation. Translation is quantified by luminescence generated by the luciferase reaction. Inhibition constants (IC_{50}) were obtained from concentration-response curves as the concentration of half-maximal inhibition of coupled transcription/translation. An additional, more stringent translation assay was performed by using an *E. coli* S30 extract, by using MS2 bacteriophage mRNA (Roche) as a template, and by measuring the incorporation of [^{3}H]methionine into peptide. High activity (+++) is defined as >75% inhibition, intermediate activity is defined as >50% inhibition, and inactive compounds as are identified by <25% inhibition at 200 μM of antibiotic concentration.

Potential inhibition of mammalian translation ("RRL IVT" for rabbit reticulocyte lysate in vitro translation) [24] is measured in an assay by using rabbit reticulocyte lysate (Promega) and the luciferase mRNA as a template for translation. As in the bacterial IVT assay, translation is quantified via luminescence generated by the luciferase reaction. Cytotoxicity (CC_{50}) is assessed by a dye reduction assay (CellTiter 96, Promega) with a HeLa cell line.

Antibacterial activity was determined by the microdilution broth method for the determination of minimum inhibitory concentration (MIC) as described [3]; Mueller-Hinton broth and *Staphylococcus aureus* ATCC 29213 were used as test organisms. MICs were defined as the lowest compound concentrations at which no visible growth occurred. An influence of the compounds on bacterial transcription and replication was excluded by pulse-labeling experiments: bacterial cells (*Staphylococcus aureus* ATCC 29213, 98 μl) were incubated in the presence of tested compound (2 μl) at a concentration corresponding to 4× the MIC value, and radioactively labeled [^{3}H]thymidine and [^{3}H]uridine (0.5 μCi/ml) were used as precursors for replication and transcription, respectively. The reaction was stopped 5 min after addition of the radioactive precursors by TCA precipitation on glass fiber filters. None of the compounds interfered with either transcription or translation.

Potential inhibition of mammalian translation (RRL IVT IC_{50}; "RRL IVT" for rabbit reticulocyte lysate in vitro translation) [24] is measured in an assay with rabbit reticulocyte lysate (Promega) and the luciferase mRNA as a template for translation. As in the bacterial IVT assay, translation is quantified via luminescence generated by the luciferase reaction. In the MS2 translation assay (Promega), incorporation of radioactive amino acid into polypeptide is measured by using *E. coli* extracts and by using MS2 phage RNA as a 13 mRNA template. This assay is generally more stringent than the *E. coli* IVT assay, and weak translation inhibitors show no activity. High activity (+++) is defined as >75% inhibition, intermediate activity is defined as >50% inhibition, and inactive compounds are identified by <25% inhibition at 200 μM antibiotic concentration. Cytotoxicity

(CC_{50}) is assessed by a dye reduction assay (CellTiter 96, Promega) with a HeLa cell line.

Computational Procedure

The X-ray structures of the complexes of the A site model with neamine and with antibiotic **3** provided the initial coordinates for the molecular dynamics simulations. The following protocol for setting up and running the molecular dynamics simulations applies to all two cases. Hydrogen atoms were added to the nucleic acid by using the "Protonate" program, which is part of the AMBER 7 [25] suite of programs. The AMBER force field parameters were assigned to all atoms by using the "parm99" set of parameters. The Sybyl 6.9 program (Tripos Inc., St. Louis, MO) was used for the manipulation and visualization of all structures and for protonation of the bound ligand. The atomic charges of the antibiotics were determined by using the RESP methodology [26]. This consisted of first optimizing the molecules at the HF/6-31G*, followed by a single-point energy calculation to determine the electrostatic potential around the molecule, which was subsequently used in the two-stage RESP fitting procedure. The Gaussian 98 package [27] was used to carry out all ab initio calculations. The program Leap was used to neutralize the complexes, and a total of 18 Na^+ ions were added to the RNA in complex with antibiotic **3**, while 20 Na^+ ions were added to the RNA-neamine complex. The complexes were immersed in a box of TIP3P [28] water molecules such that no atom in the complex was within 12 Å from any side of the box. All bonds involving hydrogen atoms were constrained by using the SHAKE [29] algorithm, and a 2 fs time step was used. The particle mesh Ewald [30] method was used to treat long-range electrostatics. Water molecules were first energy minimized and equilibrated by running a short simulation with the complex fixed by using Cartesian restraints. This was followed by a series of energy minimizations in which the Cartesian restraints were gradually relaxed from 500 kcal/Å^2 to 0 kcal/Å^2, and the system was subsequently slowly heated to 300 K via a 300 ps molecular dynamics run. Another 400 ps simulation was carried out at 300 K for further equilibration. This was followed by a 1.8 ns molecular dynamics simulation at constant pressure and temperature.

The method for determining the binding free energy has been described in the past [8, 31, 32]. It combines molecular mechanics, Poisson-Boltzmann electrostatics, surface-accessible calculations, and normal mode analyses for the entropy. These are carried out on a series of snapshots collected from a molecular dynamics simulation. The binding free energy is expressed as:

$$\Delta G_{bind} = \Delta G^{E}_{solv} + \Delta G^{L}_{solv} - \Delta G^{EL}_{solv} - \Delta G_{MM}, \quad (1)$$

where ΔG_{bind} is the binding free energy, ΔG_{MM} is the free energy of association of the enzyme and ligand in the gas phase, and ΔG^{E}_{solv}, ΔG^{L}_{solv}, and ΔG^{EL}_{solv} correspond to the solvation free energies of the A site (E), neamine or compound **3** (L), and the A site-ligand complex (EL), respectively. ΔG_{MM} is given by:

$$\Delta G_{MM} = \Delta E_{MM} - T\Delta S, \quad (2)$$

where ΔE_{MM} is the difference in the sum of bond, angle, dihedral, electrostatic, and van der Waals energies between products and reactants computed with the AMBER force field. The solvation free energy is composed of two terms, namely, electrostatics and nonpolar and is given by:

$$\Delta G_{solv} = \Delta G_{PB} + \Delta G_{nonpolar}. \quad (3)$$

In this work, 50 snapshots were collected from the aforementioned molecular dynamics simulations of antibiotic **3** and neamine bound to the A site. The electrostatic contribution to the solvation free energy is determined by using the Delphi II software package [33] that numerically solves the Poisson-Boltzmann equations to determine the electrostatic contribution to the solvation free energy. A 0.5 Å grid size was used, and the dielectric constant for the solute and solvent were set to 4 and 80, respectively. Atomic radii were taken from the PARSE parameter set, and partial charges were taken from Cornell et al. [34] for standard residues; AM1-BCC charges were assigned to neamine and antibiotic **3**. The nonpolar contribution to the solvation free energy was calculated by using the Molsurf program, which is part of the AMBER 8 suite of programs. The entropy was computed for each snapshot from normal mode analyses by using the Nmode program within the AMBER package.

Acknowledgments

The research in the USA was supported by the National Institutes of Health. We also thank the staff on ID29 at the European Synchrotron Radiation Facility for technical assistance.

Received: September 19, 2005
Revised: November 8, 2005
Accepted: November 9, 2005
Published: February 24, 2006

References

1. Knowles, D.J., Foloppe, N., Matassova, N.B., and Murchie, A.I. (2002). The bacterial ribosome, a promising focus for structure-based drug design. Curr. Opin. Pharmacol. *2*, 501–506.
2. Ramakrishnan, V. (2002). Ribosome structure and the mechanism of translation. Cell *108*, 557–572.
3. Haddad, J., Kotra, L.P., Llano-Sotelo, B., Kim, C., Azucena, E.F., Jr., Liu, M., Vakulenko, S.B., Chow, C.S., and Mobashery, S. (2002). Design of novel antibiotics that bind to the ribosomal acyltransfer site. J. Am. Chem. Soc. *124*, 3229–3237.
4. Russell, R.J., Murray, J.B., Lentzen, G., Haddad, J., and Mobashery, S. (2003). The complex of a designer antibiotic with a model aminoacyl site of the 30S ribosomal subunit revealed by X-ray crystallography. J. Am. Chem. Soc. *125*, 3410–3411.
5. Vicens, Q., and Westhof, E. (2001). Crystal structure of paromomycin docked into the eubacterial ribosomal decoding A site. Structure *9*, 647–658.
6. Wimberly, B.T., Brodersen, D.E., Clemons, W.M., Jr., Morgan-Warren, R.J., Carter, A.P., Vonrhein, C., Hartsch, T., and Ramakrishnan, V. (2000). Structure of the 30S ribosomal subunit. Nature *407*, 327–339.
7. Carter, A.P., Clemons, W.M., Brodersen, D.E., Morgan-Warren, R.J., Wimberly, B.T., and Ramakrishnan, V. (2000). Functional insights from the structure of the 30S ribosomal subunit and its interactions with antibiotics. Nature *407*, 340–348.
8. Srinivasan, J., Cheatham, T.E., III, Kollman, P.A., and Case, D.A. (1998). MMPBSA: continuum solvent studies of the stability of DNA, RNA, and phosphoramidate-DNA helices. J. Am. Chem. Soc. *120*, 9401–9409.
9. Ogle, J.M., Brodersen, D.E., Clemons, W.M., Tarry, M.J., Carter, A.P., and Ramakrishnan, V. (2001). Recognition of cognate transfer RNA by the 30S ribosomal subunit. Science *292*, 897–902.
10. Yoshizawa, S., Fourmy, D., and Puglisi, J.D. (1999). Recognition of the codon-anticodon helix by ribosomal RNA. Science *285*, 1722–1725.
11. Davies, J., Gorini, L., and Davis, B.D. (1965). Misreading of RNA codewords induced by aminoglycoside antibiotics. Mol. Pharmacol. *1*, 93–106.
12. Shandrick, S., Zhao, Q., Han, Q., Ayida, B.K., Takahashi, M., Winters, G.C., Simonsen, K.B., Vourloumis, D., and Hermann, T. (2004). Monitoring molecular recognition of the ribosomal decoding site. Angew. Chem. Int. Ed. *43*, 3177–3182.
13. Kaul, M., Barbieri, C.M., and Pilch, D.S. (2005). Defining the basis for the specificity of aminoglycoside-rRNA recognition: a comparative study of drug binding to the A sites of *Escherichia coli* and human rRNA. J. Mol. Biol. *346*, 119–134.
14. Kaul, M., Barbieri, C.M., and Pilch, D.S. (2004). Fluorescence-based approach for detecting and characterizing antibiotic-induced conformational changes in ribosomal RNA: comparing aminoglycoside binding to prokaryotic and eukaryotic ribosomal RNA sequences. J. Am. Chem. Soc. *126*, 3447–3453.
15. Banavali, N.K., and MacKerell, A.D., Jr. (2002). Free energy and structural pathways of base flipping in a DNA GCGC containing sequence. J. Mol. Biol. *319*, 141–160.
16. Foloppe, N., Chen, I.J., Davis, B., Hold, A., Morley, D., and Howes, R. (2004). A structure-based strategy to identify new

molecular scaffolds targeting the bacterial ribosomal A-site. Bioorg. Med. Chem. *12*, 935–947.
17. Clemons, W.M., Jr., Brodersen, D.E., McCutcheon, J.P., May, J.L., Carter, A.P., Morgan-Warren, R.J., Wimberly, B.T., and Ramakrishnan, V. (2001). Crystal structure of the 30S ribosomal subunit from *Thermus thermophilus*: purification, crystallization and structure determination. J. Mol. Biol. *310*, 827–843.
18. Otwinowski, Z., and Minor, W. (1997). Processing of X-ray diffraction data in oscillation mode. Methods Enzymol. *276*, 307–326.
19. CCP4 (Collaborative Computational Project, Number 4) (1994). The CCP4 suite: programs for protein crystallography. Acta Crystallogr. D Biol. Crystallogr. *50*, 760–763.
20. Brunger, A.T., Adams, P.D., Clore, G.M., DeLano, W.L., Gros, P., Grosse-Kunstleve, R.W., Jiang, J.S., Kuszewski, J., Nilges, M., Pannu, N.S., et al. (1998). Crystallography & NMR system: a new software suite for macromolecular structure determination. Acta Crystallogr. D Biol. Crystallogr. *54*, 905–921.
21. Jones, T.A., Zou, J.Y., Cowan, S.W., and Kjeldgaard, M. (1997). Acta Crystallogr. D Biol. Crystallogr. *276*, 307–326.
22. Lentzen, G., Klinck, R., Matassova, N., Aboul-ela, F., and Murchie, A.I. (2003). Structural basis for contrasting activities of ribosome binding thiazole antibiotics. Chem. Biol. *10*, 769–778.
23. Zubay, G. (1973). In vitro synthesis of protein in microbial systems. Annu. Rev. Genet. *7*, 267–287.
24. Beckler, G.S., Thompson, D., and Van Oosbree, T. (1995). In vitro translation using rabbit reticulocyte lysate. Methods Mol. Biol. *37*, 215–232.
25. Case, D.A., Pearlman, D.A., Caldwell, J.W., Cheatham, T.E., III, Wang, J., Ross, W.S., Simmerling, C.L., Darden, T.A., Merz, K.M., Stanton, R.V., et al. (2002). AMBER 7. University of California, San Francisco.
26. Bayly, C.I., Cieplak, P., Cornell, W.D., and Kollman, P.A. (1993). A well-behaved electrostatic potential based method using charge restraints for deriving atomic charges: the RESP model. J. Chem. Phys. *97*, 10269–10280.
27. Frisch, M.J., Trucks, G.W., Schlegel, H.B., Scuseria, G.E., Robb, M.A., Cheeseman, J.R., Zakrzewski, V.G., Montgomery, J.A., Jr., Stratmann, R.E., Burant, J.C., et al. (1998). Gaussian 98 and Revision A. 6. Gaussian, Inc., Pittsburgh, PA.
28. Jorgensen, W.L., Chandrasekhar, J., Madura, J.D., Impey, R.W., and Klein, M.L. (1983). Comparison of simple potential functions for simulating liquid water. J. Chem. Phys. *79*, 926–935.
29. Ryckaert, J.P., Ciccotti, G., and Berendsen, J.J.C. (1977). Numerical integration of the Cartesian equations of motion of a system with constraints: molecular dynamics of n-alkanes. J. Comput. Phys. *23*, 327–341.
30. Darden, T.A., York, D.M., and Pedersen, L.G. (1993). Particle mesh Ewald: an Nlog(N) method for Ewald sums in large systems. J. Chem. Phys. *98*, 10089–10092.
31. Massova, I., and Kollman, P.A. (2000). Combined molecular mechanical and continuum solvent approach. Perspect. Drug Discov. *18*, 113–135.
32. Wang, W., Wendell, A.L., Araz, J., Jian, W., Wang, J., Luo, R., Bayly, C.I., and Kollman, P.A. (2001). MMPBSA: an analysis of the interactions between the Sem-5 SH3 domain and its ligands using molecular dynamics, free energy calculations, and sequence analysis. J. Am. Chem. Soc. *123*, 5221–5230.
33. Nicholls, A., and Honig, B. (1991). A rapid finite-difference algorithm, utilizing successive over-relaxation to solve the Poisson-Boltzmann equation. J. Comput. Chem. *12*, 435–445.
34. Cornell, W.D., Cieplak, P., Bayly, C.I., Gould, I.R., Merz, K.M., Ferguson, D.M., Spellmeyer, D.C., Fox, T., Caldwell, J.W., and Kollman, P.A. (1995). A second generation force-field for the simulation of proteins, nucleic-acids, and organic molecules. J. Am. Chem. Soc. *117*, 5179–5197.

Accession Numbers

Coordinates have been deposited in the PDB with accession codes: 2F4T for A site antibiotic **1**, 2F4U for A site antibiotic **2**, 2F4S for neamine, and 2F4V for 30S antibiotic **1**.